THE JOURNAL OF PHYSICAL CHEMISTRY B

Article

pubs.acs.org/JPCB

Rotational and Translational Diffusion of Spin Probes in Room-Temperature Ionic Liquids

Boryana Y. Mladenova,[†] Natalia A. Chumakova,[‡] Vladimir I. Pergushov,[‡] Alexander I. Kokorin,[§] Günter Grampp,[†] and Daniel R. Kattnig*[,†]

[†]Institute of Physical and Theoretical Chemistry, Graz University of Technology, Stremayrgasse 9, A-8010 Graz, Austria

[‡]Chemical Department, Moscow State University, Moscow, Russia

[§]Institute of Chemical Physics RAS, Moscow, Russia

Supporting Information

ABSTRACT: We have studied the rotational and translational diffusion of the spin probe 4-hydroxy-2,2,6,6-tetramethyl-1-piperidinyloxy (TEMPOL) in five imidazolium-based room-temperature ionic liquids (RTILs) and glycerol by means of X-band electron paramagnetic resonance (EPR) spectroscopy. Rotational correlation times and rate constants of intermolecular spin exchange have been determined by analysis of the EPR line shape at various temperatures and spin probe concentrations. The model of isotropic rotational diffusion cannot account for all spectral features of TEMPOL in all RTILs. In highly viscous RTILs, the rotational mobility of TEMPOL differs for different molecular axes. The translational diffusion coefficients have been calculated from spin exchange rate constants. To this end, line shape contributions stemming from Heisenberg exchange and from the electron−electron dipolar interaction have been separated based on their distinct temperature dependences. While the Debye−Stokes−Einstein law is found to apply for the rotational correlation times in all solvents studied, the dependence of the translational diffusion coefficients on the Stokes parameter T/η is nonlinear; i.e., deviations from the Stokes−Einstein law are observed. The effective activation energies of rotational diffusion are significantly larger than the corresponding values for translational motion. Effects of the identity of the RTIL cations and anions on the activation energies are discussed.

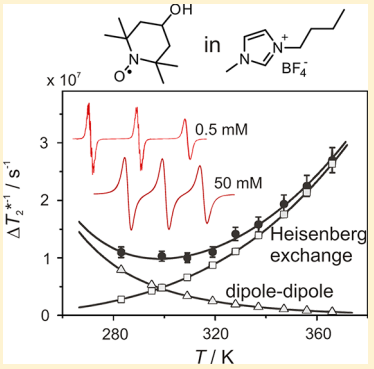

INTRODUCTION

Room-temperature ionic liquids (RTILs) are widely used as solvents for different chemical processes. Many reactions in RTILs can be carried out under milder conditions than in traditional, molecular solvents.[1,2] Furthermore, their non-volatility allows creating ecological, "green" industrial processes based on RTILs.[3,4] During the last years, there has been growing interest in the intrinsic organization and dynamics in RTILs. The diffusional processes of small molecules (reactants, additives, dopants) are of particular concern because they determine the efficiency of various chemical reactions.[5−19]

Diffusional processes of paramagnetic probe molecules can be assessed by electron paramagnetic resonance spectroscopy (EPR). The influence of the rotational tumbling of paramagnetic molecules on the width and the shape of EPR transitions is well-known.[20,21] The simulation of experimental spectra allows us to uniquely determine the rotational correlation time, τ_c (or, equivalently, the rotational diffusion coefficient/tensor D_{rot}), of probe molecules even if the molecule rotates at different rates about different axes. In addition, translational diffusional motion can be accessed by studying the line broadening resulting from Heisenberg exchange during diffusive encounters of radicals.

Many articles have been published focusing on the rotational mobility of organic molecules in RTILs as sensed by EPR spectroscopy.[8,9,12,18,22,23] The first study of rotational motion of spin labels in RTILs was published as early as 1992 by Noël et al.[22] The authors have addressed the rotational motion of TEMPO (2,2,6,6-tetramethylpiperidine-1-oxyl) and its 4-amino derivative (4-amino-TEMPO) in $AlCl_3$-containing RTILs. The larger rotational correlation time of 4-amino-TEMPO (by a factor of ca. 30 compared to TEMPO) was explained as a result of specific interactions of the RTIL ions with the NH_2 moiety.

Studying the 3-carboxy-proxyl radical in its molecular and anionic form, Miyake et al.[24] observed that the rates of rotational diffusion and the associated activation energies disagreed in [bmim$^+$][BF_4^-] and [bmim$^+$][PF_6^-] ([bmim$^+$]: 1-butyl-3-methylimidazolium cation) with those calculated from the Stokes−Einstein−Debye (SED) equation. Barrosse-Antle et al.[25] reported on the effects of halides, carbon dioxide, and water on the physical properties of [emim$^+$][$(CF_3SO_3)_2N^-$] ([emim$^+$]: 1-ethyl-3-methylimidazolium cation). The diffusion coefficients in pure and CO_2-saturated ionic

Received: July 3, 2012
Revised: August 28, 2012
Published: August 28, 2012

dx.doi.org/10.1021/jp306583g | J. Phys. Chem. B 2012, 116, 12295−12305

liquid revealed a decrease in the activation energy of translational diffusion, E^a_{tr} (from 29.0 to 14.7 kJ/mol), suggesting a reduction in the viscosity of the RTIL with CO_2 addition. EPR spectroscopy was used to determine the τ_c's of the TEMPO spin probe. Activation energies extracted from Arrhenius plots of τ_c resulted in a similar drop of E^a_{rot} (from 28.7 to 18.2 kJ/mol) for the CO_2-saturated RTIL.

The influence on the length of the alkyl chain in [1-alkyl-mim$^+$]$^+$[$(CF_3SO_3)_2N^-$] on the rotation of piperidine-1-yloxyl derivatives was reported by Strehmel et al.[9] For 4-hydroxy-2,2,6,6-tetramethyl-1-piperidinyloxy (TEMPOL), the authors observe a linear change of the rotational correlation times with RTIL viscosity. In contrast, deviations from the Stokes–Einstein–Debye behavior were found in the case of rotation of charged spin probes when the length of the 1-alkyl chain of the RTIL exceeded hexyl. It was suggested that this behavior is caused by a phase separation on a molecular level, i.e., of the charged part of the RTIL and the long alkyl chains bound to the imidazolium ions.[9] Instead of the classical SED law, the rotational diffusion coefficients of many probes have been interpreted in terms of the Gierer–Wirtz microviscosity model.[26,27]

We have recently studied the rotational dynamics of several spin probes in RTILs above room temperature. In general, the probes obeyed the SED law. However, the effective hydrodynamic radii were (too) small, even if microviscosity corrections or deviations from the idealized spherical shape of the probe molecule were taken into account.[28] Subslip behavior and a decoupling of the probe motion from solvent viscosity have also been found in fluorescence depolarization studies.[27,29,30]

The solvation of charged and uncharged nitroxide radicals in ionic liquids was studied by W- (high-field) and X-band EPR spectroscopy by Akdogan et al.[12] The authors found that the rotational motion of the charged spin probes in RTILs was about five times slower than that of TEMPOL. The change of the anion from BF_4^- to PF_6^- in the RTIL decreased the rotational mobility as well. A microstructure model of the spin probe environment was proposed. Depending on derivatization, the probes were found to be predominantly located within nonpolar domains or regions of high charge density susceptible to H-bonding. These results are in good agreement with the nanophase separation model of RTILs discussed in the literature.

We recently reported on line broadening effects caused by electron self-exchange reactions within the methyl viologene redox couple in several RTILs.[17] We have reported activation energies and compared the results to molecular solvents.[31]

Recently, Strehmel has reviewed applications of EPR to the study of RTILs. The interested reader is referred to this contribution for a more comprehensive overview of the subject.[26]

The translational diffusion coefficients, D_{tr}, of spin probes in RTILs have scarcely been studied. So far, mostly physical-chemical methods other than EPR, e.g., electrochemical methods, have been used to determine D_{tr}.[15,16] When employing EPR spectroscopy, D_{tr} values can be determined by measuring the concentration gradient of paramagnetic molecules along thin, solvent-filled tubings[18] or by the analysis of the concentration broadening of EPR spectra lines. Thereby, an approach suggested by the Freed group can be used to separate the Heisenberg exchange from dipolar broadening.[32] This method, which has not been realized for RTILs thus far, is employed here. Very recently, Stösser et al. have investigated spin-exchange effects on the EPR line shape of TEMPOL in *n*-octanol and 1-methyl-3-octylimidazolium hexafluorophosphate.[13] The authors compare several modi of data analysis, which differ predominantly in their susceptibility to interferences from electron dipole–dipole interactions. Following work by Bales, these authors suggest furthermore that, while cage and reencounter effects are relevant in both the molecular solvent and the RTIL, reencounter times are significantly larger in the RTIL.[33]

Here, we studied peculiarities of the translational and rotational diffusion of nitroxide spin probe TEMPOL in several imidazolium RTILs. The RTILs were chosen to differ in cation and anion constitution with the aim to understand the effect of the individual ions on the dynamics of small molecules.

EXPERIMENTAL SECTION

The following imidazolium-based RTILs have been used in this work: 1-ethyl-3-methylimidazolium tetrafluoroborate (IoLiTec Ionic Liquids Technologies GmbH, Germany; [emim$^+$][BF_4^-]; >98%), 1-butyl-3-methylimidazolium tetrafluoroborate (IoLiTec; [bmim$^+$][BF_4^-]; >99%), 1-octyl-3-methylimidazolium tetrafluoroborate (Solchemar, Portugal; [omim$^+$][BF_4^-]; >98%), 1-octyl-3-methylimidazolium hexafluorophosphate (Solchemar; [omim$^+$][PF_6^-]; >98%), and 1-octyl-3-methylimidazolium chloride (Fluka; [omim$^+$][Cl^-]; >97%). In addition, the following molecular solvents have been employed: toluene (ChimMed Co., Ltd.; >99.8%) and glycerol (Merck; >99%).

Toluene was dried over molecular sieves (4 Å). Glycerol was used without additional purification. To remove residual water, all RTILs were dried at elevated temperatures (313–337 K) in vacuo ($p < 5 \times 10^{-5}$ mbar) for at least 24 h. The dried RTILs were stored in Schlenk tubes under argon. The tubes were kept in the dark in a desiccator over P_4O_{10}. Samples were prepared under argon using Schlenk techniques. Note that residual water has been reported to influence the rotational motion of a selected spin probe.[28]

RTIL viscosities are summarized in Table 1 in terms of the parameters to the Vogel–Fulcher–Tammann equation

Table 1. Viscosities and Densities of the Studied RTILs[a]

solvent	E_η/K	T_0/K	η_0/mPa s	ρ/kg dm^{-3}	lit.
[bmim$^+$][BF_4^-]	907	166	0.1	1.21	61, 62
[emim$^+$][BF_4^-]	750	150	0.2	1.28	14, 63
[omim$^+$][BF_4^-]	1290	155.3	0.042	1.12	64
[omim$^+$][PF_6^-]	1450	156	0.027	1.24	64, 65
[omim$^+$][Cl^-]	–	–	–	1.01	66

[a]Viscosities are reported in terms of the interpolation parameters of eq 1. Densities are given for 293 K.

$$\eta(T) = \eta_0 \exp\left[\frac{E_\eta}{k_B(T - T_0)}\right] \quad (1)$$

Equation 1 is more flexible than the Arrhenius-type equation

$$\eta(T) = \eta_0 \exp\left[\frac{E^a_{solv}}{k_B T}\right] \quad (2)$$

which has been employed frequently to account for the temperature dependence of $\eta(T)$ of classical solvents. For the sake of comparing the activation energies of the transport

dx.doi.org/10.1021/jp306583g | J. Phys. Chem. B 2012, 116, 12295–12305

Table 2. Principal Values of *g*-Matrices and *A*-Tensors of TEMPOL in Different Ionic Liquids and Molecular Solvents[a]

solvent	g_{xx}	g_{yy}	g_{zz}	g_{iso}	A_{xx}/G	A_{yy}/G	A_{zz}/G	source
[bmim$^+$][BF_4^-]	2.0091	2.0062	2.0020	2.0058	6.8	5.6	35.0	[b]
[omim$^+$][BF_4^-]	2.0091	2.0063	2.0020	2.0058	6.3	6.1	36.0	[b]
[omim$^+$][PF_6^-]	2.0100	2.0056	2.0017	2.0058	7.1	6.2	35.6	[b]
[omim$^+$][Cl^-]	2.0094	2.0061	2.0019	2.0058	6.9	5.6	34.2	[b]
toluene	2.0094	2.0062	2.0018	2.0058	6.6	5.0	34.4	[b]
glycerol	2.0091	2.0056	2.0024	2.0057	6.9	6.6	36.5	[c]
[emim$^+$][BF_4^-]	2.00996	2.00659	2.00261	2.00639	5.7	7.2	35.1	[d]
[bmim$^+$][BF_4^-]	2.00996	2.00659	2.00258	2.00638	5.9	7.2	35.2	[e]
toluene	2.00986	2.00626	2.00222	2.00617	6.2	7.0	34.3	[f]
methanol	2.00899	2.00610	2.00218	2.00576	6.8	6.8	36.1	[f]

[a]The principal orientations of *g* and *A* have been assumed to coincide. $g_{iso} = (g_{xx} + g_{yy} + g_{zz})/3$. [b]This work. [c]This work, TEMPOL-d_{17}. [d]Private communication: Dariush Hinderberger, Max Planck Institute for Polymer Research, Mainz, Germany. [e]Ref 12. [f]Ref 67.

coefficients (D_{rot} or D_{tr}, as extracted from fits of $\ln(D)$ or $\ln(D/T)$ vs $1/T$) with the temperature dependence expected from the Stokes–Einstein or Stokes–Einstein–Debye law, the activation energies of viscous flow were calculated in the following way. The viscosities evaluated from eq 1 were fitted for the temperature range in question by the Arrhenius-type equation (eq 2). The resulting effective activation energies are reported below as E_{solv}^a.

The stable nitroxide radicals 4-hydroxy-2,2,6,6-tetramethylpiperidine-1-oxyl (Fluka; TEMPOL; ≥97%) and 4-hydroxy-2,2,6,6-tetramethylpiperidine-d_{17}-1-oxyl (Aldrich; TEMPOL-d_{17}; ≥95%, ≥97 atom % D) were employed as spin probes.

Samples were prepared gravimetrically; i.e., volumes and molar concentrations were calculated from literature densities (see Table 1). The concentration of the spin label was varied in the range from 3×10^{-4} to 5×10^{-2} M, allowing for the independent determination of τ_c (or D_{rot}) and k_e. The sample solutions were transferred into borosilicate glass capillary tubes with a bore diameter of 0.8 mm under an argon atmosphere, subject to three freeze–pump–thaw cycles, and sealed off under vacuum.

cw-EPR spectra were recorded with an X-band Bruker ELEXSYS E500 spectrometer equipped with a cylindrical TM110 cavity, a digital temperature control unit (ER4131VT), and a field-frequency lock. The sample temperature was varied from 270 to 380 ± 0.1 K in steps of 10 K. At least 10 min was allowed for thermostatting prior to each measurement. The modulation amplitude at the lowest concentrations of the spin probe was 0.05 G. The employed microwave power (0.25 mW) did not give rise to saturation broadening.

EPR spectra were simulated using Matlab in combination with the Easyspin 3.0 toolbox or home-written software. In detail, rigid-limit spectra and spectra of slow tumbling spin probes were simulated using EasySpin.[34] Spectra of spin probes subject to Heisenberg spin exchange in the fast exchange limit were modeled using home-written software based on theory outlined in ref 32. The approach has the advantage that superhyperfine interactions are rigorously taken into account. Note that depending on the relative magnitude of $|\gamma_e a_i|$ and k_e (γ_e is the gyromagnetic ratio and a_i the superhyperfine coupling constant) the broadening resulting from unresolved and partly resolved superhyperfine coupling constants will differ qualitatively and quantitatively: in the slow exchange limit (with respect to a_i, $k_e \ll |\gamma_e a_i|$), the superhyperfine pattern will give rise to an additional broadening, while in the fast exchange limit ($k_e \gg |\gamma_e a_i|$) the superhyperfine lines will collapse into a single, averaged line, and the line width directly apparent from the EPR spectrum will be close to the intrinsic line width. See ref 32 for details.

RESULTS AND DISCUSSION

Spin-Hamiltonian Parameters of TEMPOL in Ionic Liquids. Spin-Hamiltonian parameters of TEMPOL were determined by simulating rigid limit EPR spectra, recorded at 77 K. At this temperature, spin probe motions are practically frozen on the EPR time scale. Samples containing the radical at a concentration of 3×10^{-4}–5×10^{-4} mol/L were investigated in the solvents listed in Table 2. The electron dipole–dipole broadening of the EPR lines was negligible at these concentrations. Several representative EPR spectra are shown in Figure 1 overlaid by their respective computer simulations.

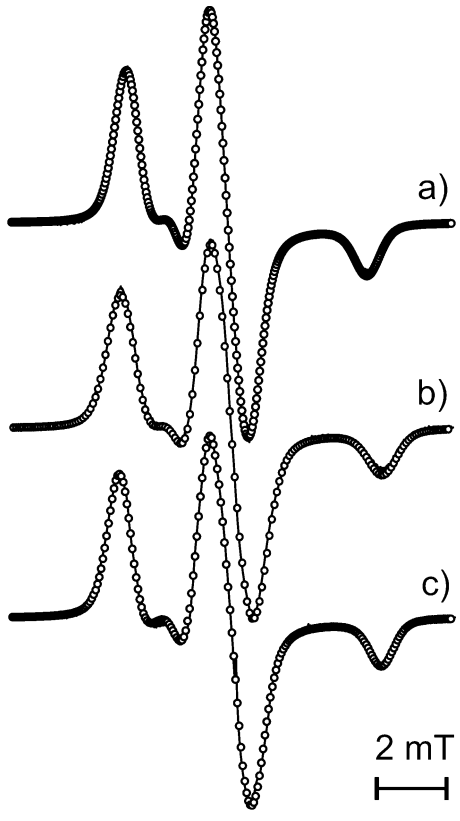

Figure 1. Experimental (solid lines) and simulated (open circles) EPR spectra of TEMPOL in frozen matrices of (a) [omim$^+$][Cl^-], (b) [bmim$^+$][BF_4^-], and (c) [omim$^+$][PF_6^-] at 77 K.

dx.doi.org/10.1021/jp306583g | J. Phys. Chem. B 2012, 116, 12295–12305

The differences between experimental and theoretical spectra are of the order of the experimental noise. Spin-Hamiltonian parameters obtained from the simulations are collected in Table 2 and compared to EPR parameters published in the literature. The average of g_{xx}, g_{yy}, and g_{zz} is reported as an isotropic g-factor (the x-axis points along the N−O bond, and the z-axis is parallel to the nitrogen p_z-orbital containing the unpaired electron density).

As can been seen from Table 2, the obtained EPR parameters correspond well with data from the literature. For the [omim$^+$]-containing RTILs, A_{zz}, a common indicator of local polarity,[12,35,36] increases in the series [omim$^+$][Cl$^-$] ∼ toluene < [omim$^+$][PF$_6^-$] < [omim$^+$][BF$_4^-$] < MeOH. In addition, the larger anisotropy of the g-matrix in the case of [omim$^+$][PF$_6^-$] in comparison with other RTILs deserves mentioning: $\Delta g = (g_{xx} - g_{yy})$ amounts to 0.0044 in [omim$^+$][PF$_6^-$], while it amounts to 0.0028 in [omim$^+$][BF$_4^-$]. This difference reflects the change in g_{xx}, which is a known gauge of hydrogen bonding and, to a lesser extent, polarity.[12,35,36] Following this notion, the observed Δg-values can probably be attributed to a less polar, less H-bonding environment of TEMPOL in [omim$^+$][PF$_6^-$] compared to the other ([omim$^+$]-containing) RTILs studied.

The temperature dependence of the *isotropic* nitrogen hfc constant, a_N, has been studied in the temperature range from 280 to 380 K. Figure 2 reproduces the dependence of a_N on T.

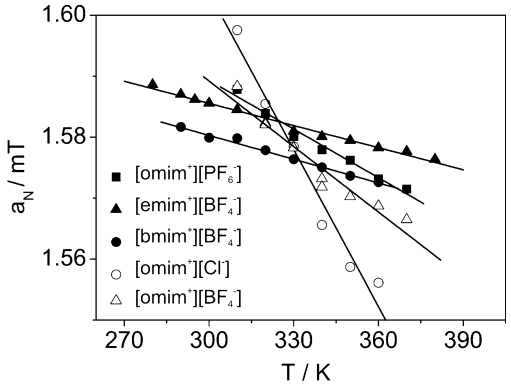

Figure 2. Temperature dependence of the nitrogen hyperfine coupling constant, a_N.

The decrease of a_N with increasing temperature is in agreement with data reported for TEMPOL in molecular solvents.[28,37,38] This temperature dependence can be interpreted in terms of nonplanarity of the nitroxide CCNO fragment and thermal averaging of the corresponding pyramidalization angle.[38] The different temperature dependences in Figure 2 suggest different strength of interaction between the probe molecules and the RTIL matrices. Notice that in the series [omim$^+$][PF$_6^-$], [omim$^+$][BF$_4^-$], and [omim$^+$][Cl$^-$] the magnitude $|da_N/dT|$ increases dramatically; see Table 3.

We speculate that this sequence reflects the electrostatic field at the surface of the anions, which makes an important contribution to the probe−matrix interaction and increases strongly with decreasing anion size. For a detailed explanation of this observation, it would be necessary to consider all direct (including hydrogen bonds) and indirect interactions of the TEMPOL molecules with the media ions. This is a very sophisticated question requiring a more detailed investigation.

Rotational Diffusion of TEMPOL Molecules. Rotational correlation times, τ_c, were extracted by means of spectral simulation of EPR spectra recorded at low probe concentrations (3×10^{-4}−5×10^{-4} M) in the temperature range from 260 to 400 K. Fast motion EPR spectra were simulated by taking all hydrogen hyperfine coupling constants of the TEMPO backbone into account. The line width and the position of the three nitrogen hyperfine lines were varied independently. $\tau_c = 1/(6\, D_{iso})$, with D_{iso} denoting the isotropic rotational diffusion coefficient, has been extracted from the homogeneous line widths using the well-known Redfield expressions.[28] Slow tumbling simulations based on the stochastic Liouville von-Neumann equation have been used to validate the applicability of the perturbation theoretical approach as well as to extract rotational correlation times at high viscosities. Freed's eigenfunction expansion approach as implemented in Easyspin 3.0 was used for this purpose.[20,34,39]

As an example, Figure 3 presents experimental EPR spectra of TEMPOL in [bmim$^+$][BF$_4^-$] recorded at different temperatures. Simulations that reproduce the data in the least-squares sense are shown as open circles. Simulated EPR spectra practically coincide with the experimental ones.

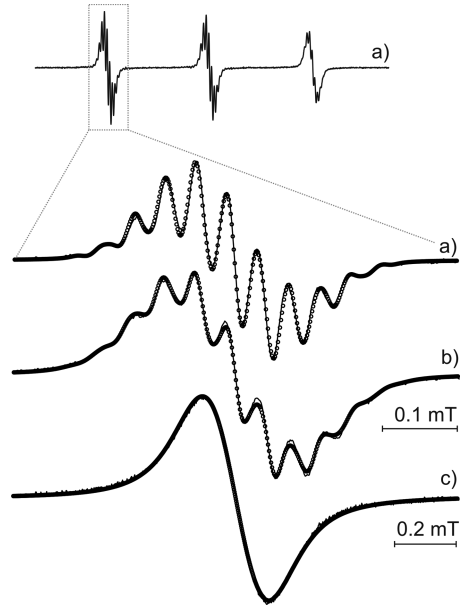

Figure 3. Experimental (solid lines) and simulated (open circles) EPR spectra of TEMPOL in [bmim$^+$][BF$_4^-$] recorded at (a) 350 K, (b) 310 K, and (c) 280 K.

In [bmim$^+$][BF$_4^-$], the rotational motion of TEMPOL is well accounted for assuming isotropic rotational diffusion. This finding is in agreement with results presented by Akdogan et al.[12] and Mladenova et al.[28] A minor improvement of the

Table 3. Temperature Coefficients of the Isotropic Nitrogen Hyperfine Coupling Constant, i.e., da_N/dT, of TEMPOL in RTILs and CCl_4

	[emim$^+$][BF$_4^-$]	[bmim$^+$][BF$_4^-$]	[omim$^+$][BF$_4^-$]	[omim$^+$][PF$_6^-$]	[omim$^+$] Cl$^-$]	[bmim$^+$][BF$_4^-$]	CCl_4
$da_N/dT/10^{-7}$ T·K^{-1}	−1.21 ± 0.05	−1.30 ± 0.15	−3.5 ± 0.40	−2.7 ± 0.2	−8.6 ± 0.8	−1.9 ± 0.2[28]	2.24[38]

dx.doi.org/10.1021/jp306583g | J. Phys. Chem. B 2012, 116, 12295−12305

spectral simulation is realized assuming an axial model of rotational diffusion with the distinguished axis parallel to the molecular x-axis, i.e., pointing in the direction of the N−O bond. With the exception of [omim$^+$][Cl$^-$], an analogous picture emerges for all RTILs studied. The rotational correlation times, $\tau_c = 1/(6\ D_{rot})$, measured at 295 K are listed in Table 4. It is obvious that τ_c, which reflects the

Table 4. Viscosities, η, Rotational Correlation Times, τ_c, Rotational Coupling Constants, c_{rot}, and Second-Order Rate Constants of Heisenberg Exchange, k_e, of TEMPOL in Different Ionic Liquids at T = 295 K[a]

solvent	η/cP	τ_c/ps	c_{rot}	k_e/L/(mol·s)
[emim$^+$][BF$_4^-$]	35[68]	130 ± 30	0.085	(1.7 ± 1.0) × 10^8
[bmim$^+$][BF$_4^-$]	123[61]	300 ± 20	0.056	(1.0 ± 0.7) × 10^8
[omim$^+$][BF$_4^-$]	417[64]	770 ± 200	0.042	(5.3 ± 0.1) × 10^7
[omim$^+$][PF$_6^-$]	923[64]	1300 ± 200	0.032	(8.2 ± 4.6) × 10^7
[omim$^+$][Cl$^-$]	20868[66]	6400 ± 800	0.007	(3.0 ± 1.0) × 10^7

[a] c_{rot} is the ratio of the diffusion coefficient calculated from eq 3 using the stick boundary condition to the experimental value. The lowest value expected for TEMPOL according to ref 41 is 0.033 (slip boundary condition).

efficiency of rotational reorientation of small probe molecules, exhibits a straightforward correlation with the dynamic viscosity, η, of the RTILs (cf. below).

For [omim$^+$][Cl$^-$], the most viscous RTIL studied here, the diffusion coefficients of rotation about the parallel (x) and the perpendicular (y and z) axes differ markedly. Figure 4 shows the Arrhenius dependences of the rotational diffusion coefficient (about different axes as well as the averaged value, $D_{av} = (D_{||}\ D_{\perp}^2)^{1/3}$) of TEMPOL in [omim$^+$][Cl$^-$].

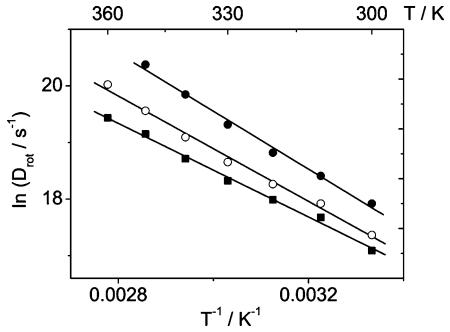

Figure 4. Rotational diffusion coefficients, D_{rot}, of TEMPOL in [omim$^+$][Cl$^-$] as a function of temperature. Solid circle refers to rotation around the x-axis and solid squares to rotation around the y- or z-axis. Open circles give the averaged rotational diffusion coefficient, D_{av}.

The slope of ln(D_{rot}) vs $1/T$ plots is proportional to the effective activation energy of the rotation process, E^a_{rot}. In [omim$^+$][Cl$^-$], the E^a_{rot} values of TEMPOL are equal to 42.6 kJ/mol for the molecular x-axis and 34.4 kJ/mol for the perpendicular axes. The average activation energy determined from D_{av} amounts to 38.7 kJ/mol. Below we shall discuss the averaged diffusion coefficient and the averaged activation energy. For the RTILs exhibiting isotropic rotational diffusion, the Arrhenius dependence of τ_c is shown in Figure 5. The effective activation energies of rotational diffusion, E^a_{rot}, have been determined by linear regression and are collected in Table 5. For comparison, the activation energies of viscous flow, E^a_{solv},

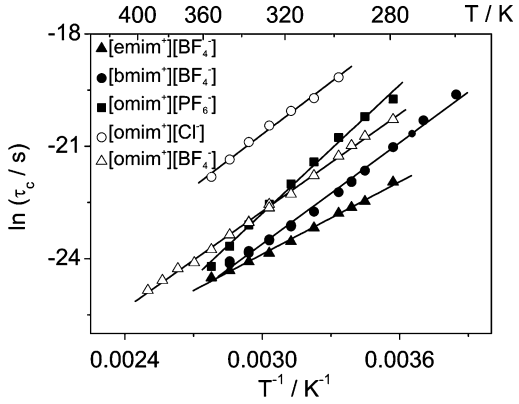

Figure 5. Arrhenius dependences of $\tau_c = 1/(6\ D_{av})$ of TEMPOL in different ionic liquids.

are also reported as well. Employing eq 2, E^a_{solv} reproduces the temperature dependence of the viscosity for the relevant temperature range.

The E^a_{rot} value for [omim$^+$][PF$_6^-$] is noticeably higher than those of the other RTILs under study. In general, the effective activation energy of viscous flow, E^a_{solv}, closely matches the activation energies of rotational diffusion, E^a_{rot} (see Table 5). In [emim$^+$][BF$_4^-$], E^a_{rot} exceeds E^a_{solv} by a small (2.8 kJ/mol), yet significant, amount, while in [omim$^+$][BF$_4^-$] it falls short of E^a_{solv} (by −2.7 kJ/mol). In view of Table 5, it should be mentioned that the pre-exponent factors reported for D_{rot}, D_{rot}^0, which are in the range of 10^{15}−10^{16} s^{-1}, are not typically related with a rotational process. Here, these values are not characteristics of an elementary process but serve the sole purpose of summarizing the rotational diffusion behavior in the indicated temperature range.

Figure 6 illustrates the dependence of $\tau_c = 1/(6\ D_{rot})$ of TEMPOL on the Stokes parameter η/T for RTILs for which the isotropic rotational diffusion model yields a satisfactory description of the experimental data. One can see that all dependences are linear; i.e., under the conditions studied the rotation of probe molecules in RTILs does not qualitatively differ from their rotation in molecular solvents and can be described by the Stokes−Einstein−Debye equation

$$D_{av} = \frac{k_B T}{6V\eta} B(p) C(p) \tag{3}$$

with k_B denoting the Boltzmann constant, T the absolute temperature, and V the hydrodynamic molecular volume, which often exceeds the molecular volume. Here, the classical SED equation has been augmented by correction factors accounting for deviations from the spherical molecular shape of the probe, $B(p)$, and slippage at the solute−solvent boundary, $C(p)$.[23,28,40,41] For spheroids with aspect ratio $p = r_{\perp}/r_{||}$, $B(p)$ is available from expression for the rotational correlation times $\tau_{||} = 1/(2D_{\perp})$ and $\tau_{\perp} = 1/(D_{\perp} + D_{||})$ derived by Perrin (taking the correction published by Koenig into account; see the cited literature for a detailed explanation).[40,42] The expression for $B(p)$ depends on how the diffusion coefficients corresponding to the unique axes, $D_{||}$ and $D_{\perp}$, are averaged to yield D_{av}. Here we follow Roosen-Runge et al. and use[43]

$$B(p) = \frac{1 + 3p^2 A(p)}{2(1 + p^2)} \tag{4}$$

with

dx.doi.org/10.1021/jp306583g | J. Phys. Chem. B 2012, 116, 12295−12305

Table 5. Parameters of Rotational and Translational Diffusion in Room Temperature Ionic Liquids and Molecular Solvents

	E_{solv}[a]	E_{rot}[a]	D_{rot}^0	E_{tr}[a]/kJ·mol^{-1}		D_{tr}^0/cm^2·s^{-1}
solvent	kJ mol^{-1}	kJ mol^{-1}	s^{-1}	from B_c	line shape simulation	from B_c
[emim$^+$][BF$_4^-$]	24	26.8 ± 0.6 (280–360 K)	6.3×10^{13}	8.4 ± 1.1 (295–380 K)	13.7 ± 0.7 (280–370 K)	6.0×10^{-6}
[bmim$^+$][BF$_4^-$]	36	37.5 ± 0.8 (260–350 K)	2.2×10^{15}	15.8 ± 1.1 (295–380 K)	17.8 ± 1.5 (290–380 K)	7.3×10^{-5}
[omim$^+$][BF$_4^-$]	39	36.1 ± 0.4 (280–400 K)	5.6×10^{14}	19.0 ± 1.2 (295–380 K)	21.7 ± 0.7 (283–366 K)	1.3×10^{-4}
[omim$^+$][PF$_6^-$]	47	47.6 ± 1.3 (280–370 K)	3.8×10^{16}	15.3 ± 1.0 (295–380 K)	17.3 ± 1.6 (300–366 K)	4.7×10^{-5}
[omim$^+$][Cl$^-$]	-	38.7 ± 1.4 (290–360 K)	1.9×10^{14}	~20 (330–366 K)	~14 (319–366 K)	1.3×10^{-4}
glycerol[a]	-	49.4 ± 0.8 (295–345 K)	4.0×10^{16}	24.1 ± 1.0 (320–380 K)		8.6×10^{-4}
cumene[48]	-	18.4 ± 0.9 (200–290 K)	1.2×10^{13}	13.4 ± 0.6 (210–360 K)		4.5×10^{-4}
n-propanol[48]	-	18.0 ± 0.6 (200–290 K)	2.4×10^{12}	20.5 ± 1.4 (220–320 K)		3.6×10^{-3}

[a]TEMPOL-d_{17}

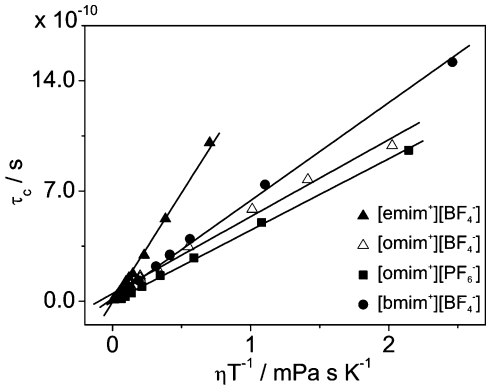

Figure 6. $\tau_c = 1/(6\ D_{av})$ of TEMPOL as a function of the Stokes–Einstein parameter, η/T, in different ionic liquids.

$$A(p) = \frac{1}{\sqrt{|1-p^2|}} \begin{cases} \tan^{-1}\left(\sqrt{p^2-1}\right) & p > 1 \text{ (oblate)} \\ \ln\left(\dfrac{1+\sqrt{1-p^2}}{p}\right) & p < 1 \text{ (prolate)} \end{cases} \quad (5)$$

This approach is based on $D_{av} = (D_{\|} + 2D_{\perp})/3$. The geometric mean, $D_{av}' = (D_{\|}D_{\perp}^2)^{1/3}$ is generally more suitable here.[21] The necessary correction factor of D_{av}' is easily calculated from the friction coefficients given by Perrin (expression given in the Supporting Information). In Figure S4 in the Supporting Information it is shown that for the aspect ratio of TEMPOL both approaches give comparable results. Note that $V = 4\pi ab^2/3 = 4\pi a^3 p^2/3$, if the hydrodynamic volume matches the molecular volume. In ref 23, the geometrical correction factor has been evaluated from Perrin's expression for $D_{\perp}$.[40,44] This result strictly applies only to $\tau_{\|}$.

We have determined the ellipsoidal parameters approximating the molecular shape by subscribing the molecular body (determined from the total electron density at a contour level of 0.02 e/Å^3) with the ellipsoid of the smallest surface area.[28] This was achieved by a constrained least-squares procedure, which optimizes the ellipsoid semiaxes, its center, and its orientation. The semiaxes obtained in this way were rescaled such that the volume of the ellipsoid matched the molecular volume (determined using a Monte Carlo approach based on the same contour of the electron density as above):[28] In good approximation, TEMPOL is represented by an oblate spheroid with the polar axes pointing along the molecular *z*-axis. $r_{\|}$ = 2.96 Å, and $r_{\perp}$ = 3.74 Å; i.e., $p = r_{\perp}/r_{\|}$ = 1.3. Note that the correction factors depend only on the aspect ratio, *p*, and not on the actual volume/radius. Thus, the geometrical correction factor according to eq 4 evaluates to $B(p = 1.3) = 0.98$. As a consequence, D_{av} calculated from eq 3 practically agrees with that calculated for a sphere of the same volume using the classical SED equation.

The correction term, $C(p)$, was introduced by Hu and Zwanzig to account for the boundary condition of momentum exchange at the solute/solvent interface.[41] For the stick boundary condition, which applies to the scenario when the solute is attached to the surrounding solvent molecules during rotation, $C_{stick} = 1$. For the slip boundary condition the tangential component of the normal stress on the surface vanishes. The correction factor, $C_{slip}(p)$, can then be obtained from Table 1 in ref (p = 1.26) = 1/0.033 by Hermite interpolation of the tabulated ratios of friction coefficients. Typically, $C(p)$ varies between C_{stick} and C_{slip}. However, subslip ($C(p) < C_{slip}$) behavior has frequently been found for spin probes in ILs.[8,9,19,23,26,28] The ratio of D_{av} was calculated from eq 3 assuming that $C = 1$, and the experimental diffusion coefficient is frequently denoted rotational coupling constant, c_{rot}.[27,29,45] This factor subsumes deviations from the stick boundary condition, departures of the hydrodynamic volume from the molecular volume, and specific interactions.[27,29,45] c_{rot} is reported in Table 4. A value of 1 and 0.033 is expected for the stick and slip boundary condition (provided the hydrodynamic volume is equal to the molecular volume). From the tabulated c_{rot} values, it is obvious that the rotational dynamics are close to the slip boundary condition and that the slippage monotonously increases with increasing viscosity. Eventually, for TEMPOL in [omim$^+$][Cl$^-$], $c_{rot} < 0.033$; i.e., the rotational dynamics are formally subslip. Thus, the hydrodynamic model breaks down, and the rotational dynamics cannot be accounted for by the model of Hu and Zwanzig.[41] Note that in

dx.doi.org/10.1021/jp306583g | J. Phys. Chem. B 2012, 116, 12295–12305

[omim$^+$][BF$_4^-$] the anisotropy of diffusion is pronounced. The orientation of the parallel axis (x) does, however, not coincide with the prediction based on molecular shape (z). This could be the result of specific solute−solvent interactions. Since for this probe/solvent system the hydrodynamic model is questionable, no clear-cut conclusions can, however, be drawn. Similar trends in c_{rot} have been observed for spin probes and fluorescence dyes.[27,29] The increasing slippage has often been attributed to an increase in the size of the solvent relative to the solute.[8,26−29] This view is consistent with the observation of comparably small c_{rot} values (large slippage) for the, relative to fluorescence probes, small spin probes. For fluorescence dyes that do not undergo specific interactions with the IL (e.g., coumarin-153), rotational dynamics are often found to lie between the stick and slip limit.[27,29,30,45] See ref 28 where this supposition is discussed in view of the Gierer−Wirtz model.[27,28,46]

Translational Mobility of TEMPOL Molecules. We have determined parameters of the translational diffusion of TEMPOL in several RTILs by measuring the concentration broadening of the EPR lines. Figure 7 shows EPR spectra of

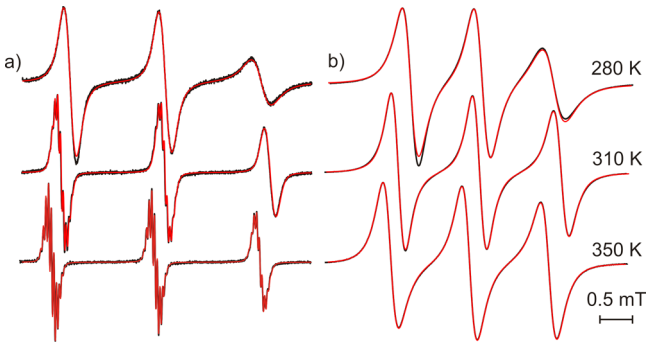

Figure 7. EPR spectra of a 0.5 mM (a) and a 50 mM (b) solution of TEMPOL in [bmim$^+$][BF$_4^-$]. From top to bottom, the temperatures are 280, 310, and 350 K. Experimental spectra (black, solid lines) are overlaid by simulations (red, solid lines) based on the formalism detailed in ref 32. This approach takes superhyperfine interactions rigorously into account.

TEMPOL at different concentrations and temperatures measured in [bmim$^+$][BF$_4^-$]. The experimental spectra are overlaid by simulations utilizing a density matrix approach.[32] Details of the simulation are discussed below. It is obvious that the spectra of the concentrated sample (b; c = 50 mM) are significantly broader than the corresponding spectra at lower radical concentrations (a; c = 0.5 mM).

At a given temperature, we have always observed a linear increase of the intrinsic (peak-to-peak) line width, ΔB_{pp}, with TEMPOL concentration. Furthermore, no spin probe dimerization or uneven distribution of radicals in the RTIL matrices became apparent; i.e., the spectra were always unimodal and of corresponding intensity. The linear increase of ΔB_{pp} with radical concentration is illustrated for selected solvents and temperatures in the Supporting Information (see Figure S1).

Here, the concentration broadening of the EPR lines originates from two causes: the modulation of the electron dipole−dipole interaction by translational diffusion and Heisenberg spin exchange. At low temperatures, when the translational motion of paramagnetic particles is significantly inhibited, the dipolar interaction between radicals is the main reason for line broadening (the most relevant relaxation term of secular origin is indirectly proportional to D_{tr}). At high temperatures, translational motion of the radicals averages their dipole−dipole interaction but, at the same time, leads to an increased frequency of spin exchange. Obviously, a temperature interval for which both contributions to the EPR line broadening are comparable in magnitude always exists. The problem of distinguishing the dipole−dipole and spin exchange contributions to the shape and width of EPR spectra lines has not been solved analytically yet.[47] However, a procedure suggested by Freed and co-workers allows estimating the contribution of both interactions and determining the effective activation energy of the translational mobility based on the analysis of the temperature dependence of the concentration broadening of EPR lines.[32] According to this procedure, the concentration broadening, B_c, may be expressed as follows

$$B_c = \Delta B_{pp}(c + c_0) - \Delta B_{pp}(c_0) = \left[a \exp\left(-\frac{E^a_{tr}}{k_B T}\right) + b \exp\left(\frac{E^a_{tr}}{k_B T}\right)\right] c \quad (6)$$

Here, E^a_{tr} is the effective activation energy of translational diffusion; c is the difference in concentrations of both radical solutions; and c_0 is the (low) concentration of the reference solution. In practice, $c_0 \approx 1 \times 10^{-4}$ M is negligible next to c. a and b are parameters, which characterize contributions of Heisenberg exchange and the dipole−dipole coupling, respectively.

The analysis of temperature dependences of concentration broadening was carried out by means of eq 6 using the method of least-squares. The parameters a and b and the effective activation energy of translational mobility, E^a_{tr}, were varied. We have approximated B_c from the difference of the peak-to-peak widths, ΔB_{pp}, of the low-field line of solutions of high and low concentrations. Note that the low- and the high-field nitrogen hyperfine lines are distorted due to the spin-exchange induced admixture of dispersion components.[47] Yet, this approach yielded smoother results than focusing on the central line. This is presumably resulting from the fact that the line is both better separated while being of comparable width as the central line. EPR spectra at low concentrations and elevated temperatures exhibit partially resolved ^{1}H-superhyperfine structure (examples shown in Figure 7a). Assuming a constant contribution of the superhyperfine structure to the broadening, the line width was still determined from the envelope of the ^{1}H-structure. Refer to ref 48 for a more detailed discussion of this approach. This simple methodology has to be regarded as approximate for the following reasons: First, the approach is applied to slow exchange only. Second, the individual transitions of the hyperfine pattern will broaden to different extents in the slow exchange limit (i.e., their statistical factors differ). Third, fast exchange may entirely average out the superhyperfine structure such that the superhyperfine broading is different at low and high concentrations. All these issues may be overcome by simulating the line shape, taking ^{1}H-superhyperfine components into account. To this end, the EPR spectra have been rigorously modeled employing a density matrix approach elaborated in ref 32. The intrinsic line width in the presence of exchange

$$T_2^{*-1} = T_2(0)^{-1} + \omega_{ex} \quad (7)$$

was then reevaluated from the fitting results (giving $T_2(0)^{-1}$ and ω_{ex}, individually). Here, $T_2(0)^{-1}$ is the relaxation rate that

dx.doi.org/10.1021/jp306583g | J. Phys. Chem. B 2012, 116, 12295−12305

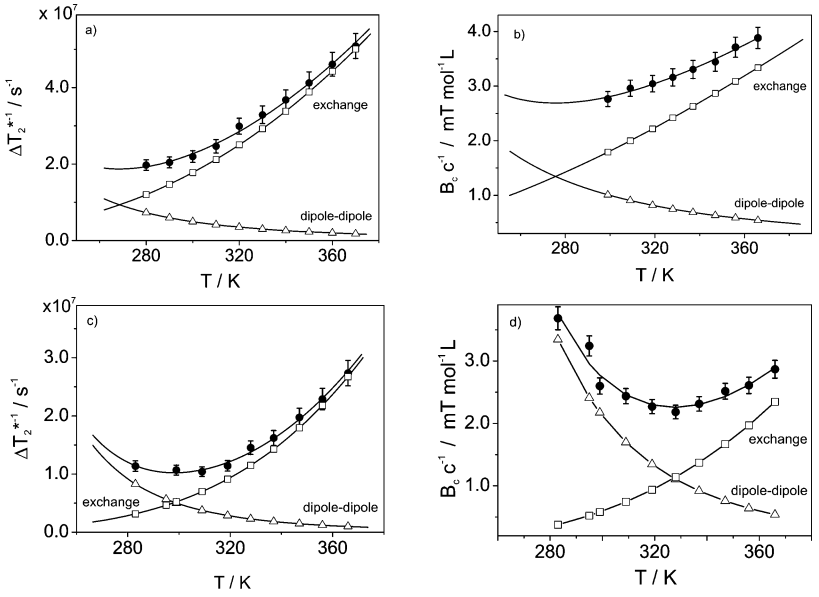

Figure 8. Differences of the intrinsic line width, $\Delta T_2^{*-1} = T_2^{*-1}(c) - T_2^{*-1}(c \approx 0, \omega_{ex} \approx 0)$, and concentration broadening (divided by concentration), B_c/c, as a function of temperature. (a) and (b) show data for TEMPOL in $[emim^+][BF_4^-]$. (c) and (d) apply to TEMPOL in $[omim^+][BF_4^-]$. The simple approach based on the apparent line width (b) and (d) underestimates E^a_{tr} and overestimates the broadening contribution of the electron dipole−dipole interaction. For (a) and (c), superhyperfine interactions have been taken into account, and the line shape has been simulated using an approach suggested in ref 32.

corresponds to the exchange-free intrinsic line width, and $\omega_{ex} = k_{ex}c$. This approach avoids the ambiguity of separating $T_2(0)^{-1}$ and ω_{ex} at low exchange rates. The temperature dependence of the difference of T_2^{*-1} at large and small radical concentrations, ΔT_2^{*-1}, was eventually analyzed by an expression analogous to eq 6. ^{1}H-hyperfine coupling constants have been taken from ref 28. Note that based on the modeling of a single spectrum the dipole−dipole and the exchange contribution can hardly be disentangled since the exchange shift of the transitions is very small.

Typical results of fitting the line broadening parameters by eq 6 are presented in Figure 8. The individual contributions of the dipole−dipole interaction, B_{dip}, and the spin exchange, B_{ex}, to the concentration broadening are indicated. Depending on the RTIL, the following three different scenarios are characteristic for the investigated temperature interval: The main contribution to the line broadening results (a) from dipole−dipole interaction ($[omim^+][Cl^-]$), (b) from the spin exchange interaction ($[emim^+][BF_4^-]$), or (c) the contributions of both of these interactions are comparable ($[omim^+][BF_4^-]$). The effective activation energies, E^a_{tr}, extracted from the temperature dependence of the line width are collected in Table 5.

To access the systematic error introduced by simply referring to the overall broadening of the EPR lines, we have compared the results of the simple approach with simulations taking superhyperfine interactions and their impact on the exchange broadening explicitly into account. In general, the simple line broadening approach underestimates E^a_{tr} (by roughly 4 kJ/mol in average). Large deviations result for $[emim^+][BF_4^-]$, the least viscous RTIL studied here, for which the activation energy E^a_{tr} differs by roughly 40% (see Table 5). Consequently, a larger dipole−dipole contribution is predicted by the simplistic line broadening approach. For $[omim^+][Cl^+]$ the results depend strongly on which spectral line is analyzed. A more detailed study will be necessary to reveal the origins of this discrepancy and to determine more accurate activation energies. The E^a_{tr} value of TEMPOL in $[omim^+][PF_6^-]$ is close to the "activation energy of spin exchange" (18.9 kJ/mol) determined by Stösser et al.[13] simulating the experimental spectra using an algorithm by Budil et al.[39] Additional experiments showed that the E^a_{tr} values are, within error margins, independent of the concentration of the spin probe. Table S1 in the Supporting Information collects E^a_{tr} of TEMPOL in $[omim^+][BF_4^-]$ determined for different concentrations from the line broadening approach.

Comparing the activation energy of translational and rotational diffusion, one realizes that the E^a_{tr} values are drastically smaller (by more than a factor of 2) than the corresponding values of $E_{rot}{}^a$, which closely match the activation energies of viscous flow, $E_{solv}{}^a$. This statement holds irrespective of the approach used for the extraction of E^a_{tr}. Note, furthermore, that except for $[omim^+][PF_6^-]$ E^a_{tr} still correlates with $E_{solv}{}^a$; i.e., larger $E_{solv}{}^a$ give rise to larger E^a_{tr}. This surprising fact will be discussed in more detail below.

Having separated the contributions of spin exchange, B_{ex}, to the concentration broadening B_c of the EPR lines, the spin exchange rate constant, k_e, is eventually calculated employing the following equation[49]

$$k_e = \frac{3^{1/2}|\gamma_e|B_{ex}}{2(1-p)c} \tag{8}$$

Here, γ_e denotes the magnetogyric ratio, and p is the fractional degeneracy of the investigated hyperfine line ($p = 1/3$ for ^{14}N-nitroxides). In a similar fashion, k_e can be determined from the simulation approach. The spin exchange rate constants determined in this way for 295 K are reported in Table 4. The k_e values obtained for TEMPOL in $[omim^+][PF_6^-]$ are close to the values reported by Stösser et al. ($k_e = 2.06 \times 10^7$−8.44×10^8 L·mol^{-1} s^{-1} at 295−372 K).[13] The error margins have been calculated by the method of error propagation.[50] It is obvious that the exchange rate constant is determined with best accuracy if the contributions of the line width originating from

dx.doi.org/10.1021/jp306583g | J. Phys. Chem. B 2012, 116, 12295−12305

spin exchange and that originating from dipolar coupling are of comparable magnitude in the studied temperature interval, i.e., when both the right and left exponential branches are accessible. The k_e's correlate with the viscosities of the RTILs except for $[omim^+][PF_6^-]$, for which the exchange rate constant k_e unexpectedly exceeds that of the less viscous $[omim^+][BF_4^-]$. This is probably indicative of pronounced re-encounter effects in the solvent cage. This suggestion is in line with previous results.[13]

For strong exchange, the spin exchange rate constant, k_e, is connected with the translational diffusion coefficient, D_{tr}, by

$$k_e = 16f\pi r D_{tr} \quad (9)$$

where f is the steric factor ($f = 0.8$ for TEMPOL)[49] and r is a radius of the paramagnetic particle. We have evaluated D_{tr} employing published data of the effective molecular size of TEMPOL ($r = 3.7$ Å).[51] Given the ansatz of eq 6, the diffusion coefficients determined in this way exhibit ideal Arrhenius behavior. The pre-exponent coefficients D^0_{tr} are summarized in Table 5. The dependence of the translational diffusion coefficient D_{tr} on the Stokes parameter, T/η, is shown in Figure 9 for three RTILs differing in the length of the alkyl

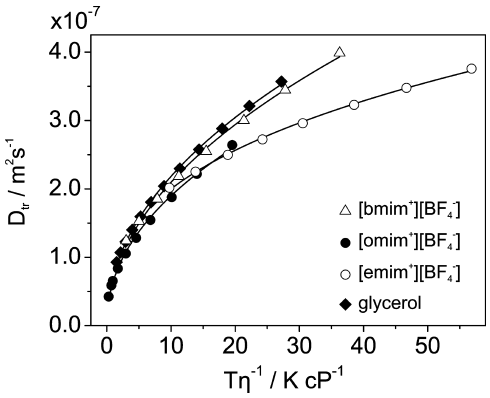

Figure 9. Diffusion coefficients of translational diffusion of TEMPOL, D_{tr}, as a function of the Stokes parameter, T/η. D_{tr} has been determined from the effective line broadening. The diffusion coefficients have been fitted assuming proportionality of D_{tr} and $(T/\eta)^x$ (solid lines). Fitting data are reported in the Supporting Information.

group of the cation and for glycerol. The dependencies of D_{tr} on T/η are similar for all RTILs studied; only for $[emim^+][BF_4^-]$ deviations from the common trend are observed. It is evident that the translational diffusion of the spin probe dissolved in RTILs cannot be described by the Stokes−Einstein equation at low temperatures, where the motion slows down considerably. This is also apparent from the observed mismatch of $E_{solv}{}^a$ and E^a_{tr}. While it has been confirmed theoretically[52] and experimentally[53−56] that imidazolium RTILs are specific media with internal structure, an explanation of our observations does not necessitate the assumption of micro-heterogeneity. In particular, we observe that a similar deviation from Stokes−Einstein behavior ensues for glycerol (to be discussed below).

In fact, some of us have previously determined E^a_{tr} and E^a_{rot} of TEMPOL dissolved in several molecular solvents using the line-broadening procedure.[48] It was revealed that for TEMPOL in cumene $E^a_{tr} < E^a_{rot}$ by approximately 25%, while in 1-propanol E^a_{tr} and E^a_{rot} were practically equal. It should be stressed that the viscosities of both cumene and 1-propanol differ strongly, i.e., by orders of magnitude, from the viscosities of the studied RTILs at the same temperature. To clarify the impact of viscosity alone, we also determined E^a_{tr} and E^a_{rot} of TEMPOL-d_{17} in glycerol, which is characterized by a viscosity comparable to that of the viscous RTILs employed here (954 mPa s at room temperature).[57]

The EPR spectra recorded at a concentration of 3×10^{-4} mol/L revealed that the rotation of the spin probe in glycerol is isotropic; i.e., the rotational reorientation proceeds with approximately the same correlation times around all three molecular axes. Figure S2 in the Supporting Information shows representative EPR spectra together with simulations based on the stochastic Liouville equation. The temperature dependence of the concentration broadening of the TEMPOL-d_{17} EPR line is shown in Figure S3 (Supporting Information). The effective rotational and translational activation energies are collected in Table 5. It turns out that the noticeable (2-fold) surplus of E^a_{rot} with respect to E^a_{tr} is not a peculiarity of ionic liquids. Apparently, the difference in activation energies observed for the translational and the rotational diffusion observed here is predominantly an effect of the high viscosity of the studied solutions.

In a recent work,[15] the effective activation energies of the rotational and translational movements of the TEMPO radical (2,2,6,6-tetramethylpiperidine-1-oxyl) dissolved in several RTILs of the alkylammonium type were determined. The rotational mobility parameters obtained by Evans et al.[15] were determined by EPR spectroscopy, while the translational characteristics were calculated from electrochemical experiments. In this study, E^a_{tr} values were comparable or by up to 25% larger than the corresponding E^a_{rot} values for all RTILs studied. Comparing the results of Evans et al. with ours, we conclude that electron spin exchange in viscous media does not only reflect the translational mobility of the paramagnetic molecules but also is sensitive to processes which take place within the "solvent cage". Probably the paramagnetic molecules undergo a repeated spin exchange process before they eventually escape the cage. Such processes are discussed in detail in a series of publications.[58−60] These authors calculate the time of re-encounter on the basis of a relationship of the hyperfine spacing and the broadening of the spectral lines. A linear correlation between rotational correlation time and re-encounter time was shown. The encounter time of two probe molecules inside the cage of highly viscous solvent is longer than in low-viscosity solvent, such that the contribution of recollisions to spin exchange is larger. Obviously the activation energy of re-encounters is much smaller than the activation energy of macroscopic translational diffusion. For this reason, the effective activation energy defined on the basis of spin exchange in very viscous media is smaller than the activation energy of macroscopic translational diffusion. Further experiments including the determination of effective activation energies of the translational and rotational diffusion in RTILs and other viscous solvents by different physicochemical methods have to be undertaken to eventually confirm this supposition.

CONCLUSION

The rotational and translational diffusion of TEMPOL has been studied in a series of room-temperature ionic liquids using EPR spectroscopy. Rotational correlation times and rotational diffusion coefficients, as well as spin exchange rate constants

and translational diffusion coefficients, were determined at different temperatures. The correlation of the measured parameters with the solvent viscosity has been established. It was shown that the rotational diffusion of the small molecule TEMPOL dissolved in RTILs is in good agreement with the Debye−Stokes−Einstein law, while the translational diffusion of the probe deviates substantially from the Stokes−Einstein law at temperatures below 330 K. The rotational boundary condition is close to the slip limit. The rotational coupling constant decreases with increasing viscosity. For $[omim^+][Cl^-]$ the behavior is subslip. The effective activation energies of rotational (E^a_{rot}) and translational (E^a_{tr}) diffusion have been evaluated. E^a_{tr} has been measured from the concentration broadening of the EPR lines. The broadening resulting from Heisenberg spin exchange has been separated from the dipole−dipole broadening utilizing the temperature dependence of the intrinsic line width. In all RTILs studied, and also in the viscous molecular solvent glycerol, the E^a_{rot} values exceed the E^a_{tr} values, calculated from the spin exchange rate constants, significantly. We attribute this observation to repeated reencounters of the spin probe within the solvent cage. Isoviscous studies are mandatory to elucidate the peculiarities of ILs and distinguish them from mere effects of the large viscosities. This not only applies to EPR but also is a general recommendation. A similar conclusion was recently drawn in a photophysical study.[30]

■ ASSOCIATED CONTENT

Supporting Information

A) Peak-to-peak line width of the central EPR transition of TEMPOL in $[omim^+][BF_4^-]$ and glycerol as a function of TEMPOL concentration. B) Dependence of the activation energy of the translational diffusion of TEMPOL on the spin probe concentration. C) EPR spectra of TEMPOL-d_{17} in glycerol at various temperatures. D) Temperature dependence of the concentration broadening of the EPR lines of TEMPOL-d_{17} in glycerol and its decomposition in contributions ascribed to Heisenberg exchange and the electron dipole−dipole interaction. E) Geometry correction factors for ellipsoidal molecules based on Perrin's expressions. F) Empirical representations of the translational diffusion coefficients by fractional Stokes−Einstein equations. This material is available free of charge via the Internet at http://pubs.acs.org.

■ AUTHOR INFORMATION

Corresponding Author

*E-mail: daniel.kattnig@tugraz.at.

Notes

The authors declare no competing financial interest.

■ ACKNOWLEDGMENTS

The authors thank Prof. A. Kh. Vorobiev and Prof. M. Ya. Melnikov for fruitful discussions and the Russian Foundation for Basic Research (Grants 08-03-00478 and 12-03-00623_a) for financial support.

■ REFERENCES

(1) Kokorin, A. *Ionic liquids: applications and perspectives*; Intech: Rijeka, 2011.
(2) Dyson, P. J.; Geldbach, T. J. *Metal catalysed reactions in ionic liquids*; Springer: Dordrecht, 2005.
(3) Rogers, R. D.; Seddon, K. R. *Ionic liquids: industrial applications for green chemistry*; Oxford University Press: Oxford, 2002.
(4) Earle, M. J.; Seddon, K. R. *Pure Appl. Chem.* **2000**, *72*, 1391−1398.
(5) Weingärtner, H. *Angew. Chem., Int. Ed.* **2008**, *47*, 654−670.
(6) Baker, S. N.; Baker, G. A.; Kane, M. A.; Bright, F. V. *J. Phys. Chem. B* **2001**, *105*, 9663−9668.
(7) Ito, N.; Richert, R. *J. Phys. Chem. B* **2007**, *111*, 5016−5022.
(8) Stoesser, R.; Herrmann, W.; Zehl, A.; Strehmel, V.; Laschewsky, A. *ChemPhysChem* **2006**, *7*, 1106−1111.
(9) Strehmel, V.; Rexhausen, H.; Strauch, P. *Phys. Chem. Chem. Phys.* **2010**, *12*, 1933−1940.
(10) Mandal, P. K.; Saha, S.; Karmakar, R.; Samanta, A. *Curr. Sci.* **2006**, *90*, 301−310.
(11) Ingram, J. A.; Moog, R. S.; Ito, N.; Biswas, R.; Maroncelli, M. *J. Phys. Chem. B* **2003**, *107*, 5926−5932.
(12) Akdogan, Y.; Heller, J.; Zimmermann, H.; Hinderberger, D. *Phys. Chem. Chem. Phys.* **2010**, *12*, 7874−7882.
(13) Stösser, R.; Herrmann, W.; Marx, U.; Brückner, A. *J. Phys. Chem. A* **2011**, *115*, 2939−2952.
(14) Noda, A.; Hayamizu, K.; Watanabe, M. *J. Phys. Chem. B* **2001**, *105*, 4603−4610.
(15) Evans, R. G.; Wain, A. J.; Hardacre, C.; Compton, R. G. *ChemPhysChem* **2005**, *6*, 1035−1039.
(16) Matsumiya, M.; Terazono, M.; Tokuraku, K. *Electrochim. Acta* **2006**, *51*, 1178−1183.
(17) Grampp, G.; Kattnig, D.; Mladenova, B. *Spectrochim. Acta, Part A: Mol. Biomol. Spectrosc.* **2006**, *63*, 821−825.
(18) Stoesser, R.; Herrmann, W.; Zehl, A.; Laschewsky, A.; Strehmel, V. *Z. Phys. Chem.* **2006**, *220*, 1309−1342.
(19) Strehmel, V.; Rexhausen, H.; Strauch, P.; Strehmel, B. *ChemPhysChem* **2010**, *11*, 2182−2190.
(20) Freed, J. H.; Fraenkel, G. K. *J. Chem. Phys.* **1963**, *39*, 326−348.
(21) Schneider, D. J.; Freed, J. H. Berliner, L. J.; Reuben, J., Eds.; *Biological magnetic resonance*; Plenum Publishing Corporation: New York, 1989; Vol. *8*, pp 1−76.
(22) Noel, M. A. M.; Allendoerfer, R. D.; Osteryoung, R. A. *J. Phys. Chem.* **1992**, *96*, 2391−2394.
(23) Miyake, Y.; Akai, N.; Kawai, A.; Shibuya, K. *J. Phys. Chem. A* **2011**, *115*, 6347−56.
(24) Miyake, Y.; Hidemori, T.; Akai, N.; Kawai, A.; Shibuya, K.; Koguchi, S.; Kitazume, T. *Chem. Lett.* **2009**, *38*, 124−125.
(25) Barrosse-Antle, L. E.; Hardacre, C.; Compton, R. G. *J. Phys. Chem. B* **2009**, *113*, 2805−2809.
(26) Strehmel, V. *ChemPhysChem* **2012**, *13*, 1649−1663.
(27) Das, S. K.; Sarkar, M. *ChemPhysChem* **2012**, *13*, 2761−8.
(28) Mladenova, B. Y.; Kattnig, D. R.; Grampp, G. *J. Phys. Chem. B* **2011**, *115*, 8183−8198.
(29) Das, S. K.; Sarkar, M. *J. Phys. Chem. B* **2012**, *116*, 194−202.
(30) Khara, D. C.; Samanta, A. *Phys. Chem. Chem. Phys.* **2010**, *12*, 7671−7677.
(31) Grampp, G.; Mladenova, B. Y.; Kattnig, D. R.; Landgraf, S. *Appl. Magn. Reson.* **2006**, *30*, 145−164.
(32) Nayeem, A.; Rananavare, S. B.; Sastry, V. S. S.; Freed, J. H. *J. Chem. Phys.* **1989**, *91*, 6887−6905.
(33) Bales, B. L.; Peric, M. *J. Phys. Chem. B* **1997**, *101*, 8707−8716.
(34) Stoll, S.; Schweiger, A. *J. Magn. Reson.* **2006**, *178*, 42−55.
(35) Steinhoff, H.-J.; Savitsky, A.; Wegener, C.; Pfeiffer, M.; Plato, M.; Möbius, K. *Biochim. Biophys. Acta, Bioenerg.* **2000**, *1457*, 253−262.
(36) Plato, M.; Steinhoff, H.-J.; Wegener, C.; Törring, J. T.; Savitsky, A.; Möbius, K. *Mol. Phys.* **2002**, *100*, 3711−3721.
(37) Kokorin, A. I. *Appl. Magn. Reson.* **2004**, *26*, 253−274.
(38) Bullock, A. T.; Howard, C. B. *J. Chem. Soc., Faraday Trans. 1* **1980**, *76*, 1296−1300.
(39) Budil, D. *J. Magn. Reson. A* **1996**, *120*, 155−189.
(40) Perrin, F. *J. Phys. Radium* **1934**, *5*, 497−511.
(41) Hu, C.-M.; Zwanzig, R. *J. Chem. Phys.* **1974**, *60*, 4354−4357.
(42) Koenig, S. H. *Biopolymers* **1975**, *14*, 2421−2423.
(43) Roosen-Runge, F.; Hennig, M.; Zhang, F.; Jacobs, R. M.; Sztucki, M.; Schober, H.; Seydel, T.; Schreiber, F. *Proc. Natl. Acad. Sci. U.S.A.* **2011**, *108*, 11815−20.

(44) Roy, M.; Doraiswamy, S. *J. Chem. Phys.* **1993**, *98*, 3213−3223.
(45) Das, S. K.; Sarkar, M. *Chem. Phys. Lett.* **2011**, *515*, 23−28.
(46) Gierer, A.; Wirtz, K. *Z. Naturforsch.* **1953**, *A8*, 532−538.
(47) Salikhov, K. M. *Appl. Magn. Reson.* **2010**, *38*, 237−256.
(48) Chumakova, N. A.; Pergushov, V. I.; Vorobiev, A. K.; Kokorin, A. I. *Appl. Magn. Reson.* **2010**, *39*, 409−421.
(49) Molin, Y.; Salikhov, K. M.; Zamaraev, K. I. *Spin exchange*; Springer-Verlag: Berlin, NY, 1980.
(50) Gordon, A. J.; Ford, R. A. *The chemist's companion: a handbook of practical data, techniques, and references*; Wiley: New York, 1972.
(51) Kokorin, A. I. *Methods of Spin Labels and Probes: Problems and Perespectives*; Nauka: Moscow, 1986, 61−79.
(52) Wang, Y.; Voth, G. A. *J. Phys. Chem. B* **2006**, *110*, 18601−18608.
(53) Triolo, A.; Russina, O.; Bleif, H.-J.; Di Cola, E. *J. Phys. Chem. B* **2007**, *111*, 4641−4644.
(54) Iwata, K.; Okajima, H.; Saha, S.; Hamaguchi, H. *Acc. Chem. Res.* **2007**, *40*, 1174−1181.
(55) Xiao, D.; Hines, L. G.; Bartsch, R. A.; Quitevis, E. L. *J. Phys. Chem. B* **2009**, *113*, 4544−4548.
(56) Hu, Z.; Claudio, J. M. *Proc. Natl. Acad. Sci. U.S.A.* **2006**, *103*, 831−836.
(57) Haynes, W. M. *CRC handbook of chemistry and physics*; CRC, Taylor & Francis: Boca Raton, FL; London, 2011.
(58) Kurban, M. R.; Peric, M.; Bales, B. L. *J. Chem. Phys.* **2008**, *129*, 064501.
(59) Kurban, M. R. *J. Chem. Phys.* **2009**, *130*, 104502.
(60) Kurban, M. R. *J. Chem. Phys.* **2011**, *134*, 034503.
(61) Harris, K. R.; Kanakubo, M.; Woolf, L. A. *J. Chem. Eng. Data* **2007**, *52*, 2425−2430.
(62) Rebelo, L. P. N.; Najdanovic-Visak, V.; Visak, Z. P.; Nunes da Ponte, M.; Szydlowski, J.; Cerdeirina, C. A.; Troncoso, J.; Romani, L.; Esperanca, J. M. S. S.; Guedes, H. J. R.; de Sousa, H. C. *Green Chem.* **2004**, *6*, 369−381.
(63) Noda, A.; Hayamizu, K.; Watanabe, M. *J. Phys. Chem. B* **2001**, *105*, 4603−4610.
(64) Harris, K. R.; Kanakubo, M.; Woolf, L. A. *J. Chem. Eng. Data* **2006**, *51*, 1161−1167.
(65) Sanmamed, Y.; Gonzalezsalgado, D.; Troncoso, J.; Cerdeirina, C.; Romani, L. *Fluid Phase Equilib.* **2007**, *252*, 96−102.
(66) Calvar, N.; Gómez, E.; González, B.; Domínguez, Á. *J. Chem. Eng. Data* **2007**, *52*, 2529−2535.
(67) Lebedev, Y. S.; Grinberg, O. Y.; Dubinsky, A. A.; Poluektov, O. G. In: *Bioactive spin labels*; Zhdanov, R. I., Ed.; Springer-Verlag: Berlin, Heidelberg, 1992; pp 228−254.
(68) Jacquemin, J.; Husson, P.; Padua, A. A. H.; Majer, V. *Green Chem.* **2006**, *8*, 172−180.